How to better focus waves by considering symmetry and information loss

Kai Lou[a], Steve Granick[a,b,1], and François Amblard[a,c,d,1]

[a]Center for Soft and Living Matter, Institute for Basic Science, Ulsan 44919, South Korea; [b]Department of Chemistry, Ulsan National Institute of Science and Technology, Ulsan 44919, South Korea; [c]Department of Physics, Ulsan National Institute of Science and Technology, Ulsan 44919, South Korea; and [d]School of Life Sciences, Ulsan National Institute of Science and Technology, Ulsan 44919, South Korea

Contributed by Steve Granick, May 9, 2018 (sent for review March 2, 2018; reviewed by Jörg Enderlein and Hervé Rigneault)

We amend the general belief that waves with extended spherical wavefront focus at their center of curvature. Instead, when the spherical symmetry of waves is broken by propagating them through a finite aperture along an average direction, the forward/backward symmetry is broken and the focal volume shifts its center backward along that direction. The extent of this focal shift increases as smaller apertures are used, up to the point that the nominal focal plane is out of focus. Furthermore, the loss of axial symmetry with noncircular apertures causes distinct focal shifts in distinct axial planes, and the resulting astigmatism possibly degrades the axial focusing resolution. Using experiments and simulations, focal shift with noncircular apertures is described for classical and temporal focusing. The usefulness of these conclusions to improve imaging resolution is demonstrated in a high-resolution optical microscopy application, namely line-temporal focusing microscopy. These conclusions follow from fundamental symmetries of the wave geometry and matter for an increasing number of emerging optical techniques. This work offers a general framework and strategy to understand and improve virtually any wave-based application whose efficacy depends on optimal focusing and may be helpful when information is transmitted by waves in applications from electromagnetic communications, to biological and astronomical imaging, to lithography and even warfare.

diffraction theory | focal shift | imaging | two-photon microscopy | spatiotemporal focusing

If the arrow of time could be reversed, our intuition is that waves from a pebble dropped into a pond would reverse direction and refocus at the precise impact point. But if the source of time-reversed waves is limited to just a portion of the pond periphery, information is lost, the circular symmetry is broken, and back-propagating waves are no longer expected to refocus at the same point (Fig. 1*A*). This simple 2D argument can be extended for 3D spherical waves propagating from and toward their geometric center, i.e., the center of curvature of the wave fronts. Obviously, the spherical symmetry of the focused field breaks down if the wavefronts occupy less than the full-space 4π solid angle. More precisely, if a wave comes with a main propagation direction, the forward–backward reversal symmetry along that axis is broken. Since that case represents practically all wave-focusing situations, the usual expectation that the intensity is symmetric relative the focal plane is no longer self-evident.

This first simple symmetry argument leads to the notion that the intensity distribution could possibly shift along the focusing axis, depending on the extent of forward–backward symmetry breaking, i.e., on the aperture angle. As intuitive as it sounds, this possibility is rarely considered for focused waves in general, regardless of their nature. Instead, for electromagnetic, acoustic, or matter waves with spherical wavefronts, one generally presumes that the center of the focal volume sits at the geometric center of those waves. This general viewpoint is consistent with the framework derived from the landmark contributions of Wolf (1) and Richards and Wolf (2), which has proved accurate and tremendously useful for decades in the field of optics for most light-focusing applications. Nevertheless, as discussed in more detail in *Historical Context*, this viewpoint has been challenged both experimentally and theoretically since the late 1950s and early 1960s (3), by the introduction of the concept of focal shift: The axial intensity distribution peaks at a point that increasingly shifts toward the focus for smaller Fresnel numbers. The Fresnel number is a dimensionless number, $\mathcal{N}=a^2/\lambda f$, which reflects the relative contribution of focusing vs. diffraction effects for a given aperture radius a, focal length f, and wavelength λ. This retrograde shift phenomenon has been observed in a small number of experimental reports with Gaussian beams and spherical waves (4–7) and explained through a much larger series of analytical or numerical studies (3, 4, 8–15).

The concept of focal shift has been to a very large extent disregarded in the field of wave focusing in general, most likely for practical reasons. Not only does the amplitude of the shift rapidly vanish for large Fresnel numbers, with virtually no effect for focusing applications with large apertures, but also axial shifts can be caused and are in general thought to be solely the result of geometric aberrations of the focusing devices. Instead, the notion of focal shift discussed here is an intrinsic property of the wave, not of the focusing device. In recent years, a number of techniques using microlenses or metamaterials-based focusing devices have emerged, in which focal shift matters because they combine large-aperture angles with small Fresnel numbers (15–19).

In the present work, we experimentally explore the concept of optical focal shift for apertures and beams with noncircular symmetry and relatively large Fresnel numbers ($\mathcal{N}>100$). We first provide simple physical symmetry arguments strongly suggesting

Significance

With applications from electromagnetic communications, to biological and astronomical imaging, to lithography and warfare, waves transmit information, and optimal wave focusing is essential. Here we demonstrate the need to amend the belief that spherical or cylindrical wavefronts necessarily focus at their center of curvature. Instead the effective focus shifts toward the source with decreasing apertures, producing astigmatism when, as increasingly shown for modern applications, the wavefronts are not axially symmetric. This leads to significant degradation of axial resolution in nonaxisymmetric light-focusing applications. These conclusions, derived from diffraction theory and validated by application to optical bioimaging, offer a general strategy to likewise improve the resolution of virtually any other wave-based application whose efficacy depends on focusing energy to points or lines.

Author contributions: K.L. and F.A. designed research; K.L. and F.A. performed research; K.L., S.G., and F.A. analyzed data; and K.L., S.G., and F.A. wrote the paper.

Reviewers: J.E., University of Göttingen; and H.R., Institut Fresnel.

The authors declare no conflict of interest.

[1]To whom correspondence may be addressed. Email: famblard@protonmail.com or sgranick@ibs.re.kr.

This article contains supporting information online at www.pnas.org/lookup/suppl/doi:10.1073/pnas.1803652115/-/DCSupplemental.

Published online June 13, 2018.

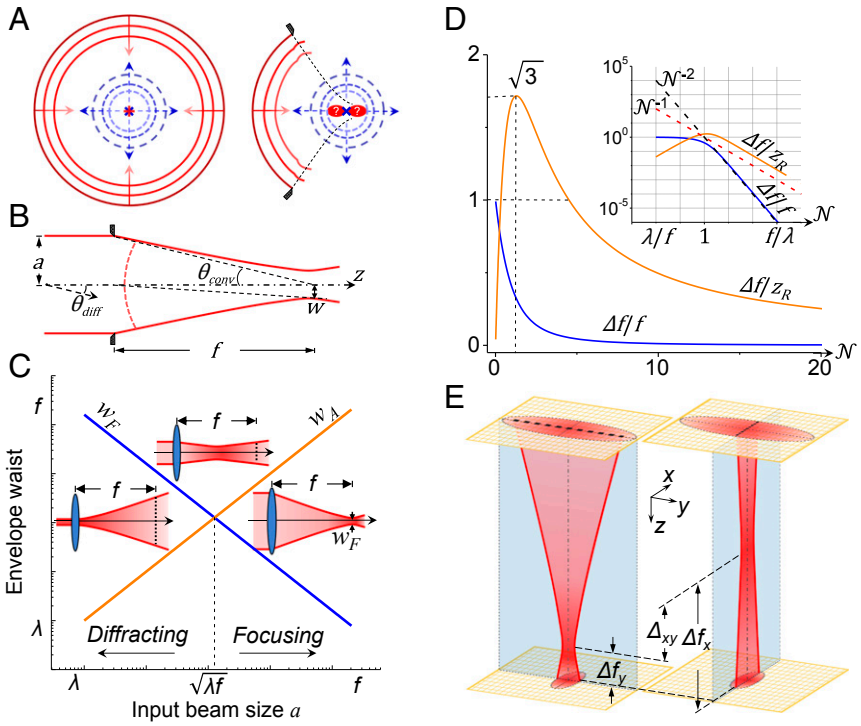

Fig. 1. Information loss, focal shift, and aperture-induced astigmatism. (*A*) Schematic 2D depiction of time-reversed spherical waves and how the use of a limited aperture breaks the spherical symmetry, leading to the possibility that the focus no longer sits at the center of curvature of wavefronts. (*B*) Wave focused through aperture 2*a* with convergence angle θ_{conv} and diffraction angle θ_{diff}. (*C*) Envelope of the energy flow, converging or diverging for large or small apertures. (*D*) Focal shift Δf computed from the scalar diffraction integral in the Fresnel approximation, relative to the focal length f and the depth of focus (Rayleigh length z_R). $\mathcal{N} = \theta_{conv}/\theta_{diff}$ is the Fresnel number. (*E*) Astigmatism produced by a noncircular aperture, with a gap Δf_{xy} between shifted focal planes.

that the focus must shift backward for Fresnel numbers close to unity, thus leading to astigmatic focusing when the circular symmetry of the input light beam is broken. Focal shift is measured in such asymmetric conditions, as well as for the temporal focusing of femtosecond pulses. As a practical consequence, we finally show a significant improvement of the axial resolution of line-temporal focusing microscopy, a high-end nonlinear microscopy method recently developed for high-resolution, high-speed in-depth optical imaging.

Why the Focus Must Shift Backward

If we consider spherical wavefronts propagating from a circular aperture (aperture radius a, focal length f, wavelength λ), the focusing efficiency trades off between convergence and diffraction controlled by the dimensionless parameters $\theta_{conv} = a/f$ and $\theta_{diff} = \lambda/a$ (Fig. 1*B*), respectively. When the aperture decreases from large to very small values ($a \sim f$ to $a \to \lambda$), the energy flow carried by the wave evolves from a converging to a diverging shape. Following previous analyses (5, 14, 20), one can define the envelope that encircles a finite proportion (e.g., 50%) of the energy flow, i.e., the 2D manifold which is tangential to the Poynting vector field (Fig. 1*C*). The waist of that envelope in the aperture and the focal planes, w_A and w_F, respectively, evolves from $w_F \ll w_A \sim a$ to $w_F \gg w_A \sim a$. Qualitatively, a critical situation must therefore occur in which w_F and w_A cross, when diffraction and focusing balance each other, i.e., for a critical aperture radius $a = a_c \sim \sqrt{\lambda f}$. Let us now consider its shape in this critical situation under the assumption that $\lambda \ll f$. Close to the aperture plane, because of the latter assumption, $a_c \gg \lambda$ and the field away from the aperture boundary is dominated by the spherical wavefront. As a result, the Poynting vector necessarily bends toward the axis, and the waist of the energy envelope must first decrease before it increases again to meet the critical condition. In other words, a region must exist between the aperture and the focal planes where the energy flow inside the envelope is more concentrated than in the extreme planes. Therefore, the transverse plane of maximum energy concentration shifts toward the lens (*SI Appendix*, Fig. S1). Since this argument does not depend on any specific property of light, it is expected to apply generally to all waves. Two seemingly equivalent definitions of the focal plane can in principle be considered (14) (*SI Appendix*, section *a*), based either on the transverse energy concentration or on the position of the axial intensity peak. The latter definition is traditionally used in this field, because it is more practical for both theory and experiences, and it is used in this paper from now on.

Scaling Analysis of the Focal Shift Effect

To estimate the practical consequences of this focal shift, its magnitude Δf was computed here using the scalar diffraction integral, with the paraxial and Fresnel approximations for Gaussian, but without the usual linearization of the pupil phase function, and for a wide range of Fresnel numbers $\mathcal{N} = \theta_{conv}/\theta_{diff}$ (14) (*SI Appendix*, section *b*). Plots of the focal shift relative to the focal length f and the Rayleigh length Z_R as a function of the Fresnel number $\mathcal{N}$ (Fig. 1*D*) show that $\Delta f/f$ decreases as $\mathcal{N}^{-2} \propto a^{-4}$ for increasing $\mathcal{N}$. For $\mathcal{N} \approx 1.1$, $\Delta f/f \sim 0.4$ and the ratio $\Delta f/Z_R$ reaches maximum ($\sqrt{3}$), meaning that the nominal focal plane is effectively out of focus. However, when $a \to f$ at the upper boundary of the paraxial approximation domain, conventional findings are recovered: $\Delta f/Z_R$ scales as $\mathcal{N}^{-1} \propto a^{-2}$, and the nominal focal plane remains in focus. The shift can be safely neglected compared with the focal length and the depth of focus, as long as such large-aperture angles correspond to large Fresnel numbers.

Practically, focal shift should be considered when focusing from circular apertures with low Fresnel number ($\mathcal{N} \leq 100$) for imaging applications such as highly inclined laminated optical sheet (HiLo) (21), total internal reflection fluorescence (TIRF) (22), multifocus versions of stimulated emission depletion (STED) nanoscopy (23), RESOLFT (REversible Saturable Optical Linear Fluorescence Transitions) nanoscopy (19), and near-field focusing with microlenses (16) or plasmonic lenses (18). It is important to note that large-aperture angle situations can unexpectedly correspond to small Fresnel number values, when both the aperture and the focal length are small, e.g., such that $1 < a/\lambda < 10$ and $1 < f/\lambda < 10$ (15, 24).

Astigmatic Focal Shift Expected for Noncircular Apertures

To the best of our knowledge, focal shift of 3D waves has been studied only experimentally for circular apertures or circular Gaussian beams (4–7). In the noncircular case, one can obviously

no longer use a single Fresnel number, and theoretical reports describe how the axial intensity distribution can be computed from two Fresnel numbers, as first introduced for Gaussian elliptical beams (25). It is our purpose here to investigate experimentally the axial intensity profile when the circular symmetry of the aperture or the field is broken. Qualitatively, one expects the loss of the circular symmetry to break the axial symmetry of the intensity in the focal region. As a consequence, one expects the above energy envelope to assume a pseudoastigmatic shape, with distinct focal shifts in the xz and yz axial planes, and a gap between them, $\Delta_{xy} = \Delta f_y - \Delta f_x$ (Fig. 1*E*). This remark leads to the notion that a perfectly spherical wave should generate astigmatic focusing as a consequence of a noncircular aperture and that a collimated elliptical beam focused through an aberration-free spherical lens should behave similarly. It also leads to the possibility that the axial intensity distribution could be stretched because of a focal shift gap. These original qualitative predictions need to be experimentally tested and their outcome may matter for optical microscopies such as light-sheet microscopy (26), temporal focusing microscopy (27, 28), light-gradient applications (29, 30), and optical lithography, as well as for acoustic waves or electron beams.

Experimentally, we studied the effect of aperture asymmetry, using a microscope objective lens with back aperture diameter $2R$, together with an elliptical Gaussian beam characterized by two effective Fresnel numbers. These numbers, $\mathcal{N}_x = a_x^2/\lambda f$ and $\mathcal{N}_y = a_y^2/\lambda f$, are defined from the beam radii a_x and a_y, while $\alpha_x = a_x/R$ and $\alpha_y = a_y/R$ are the aperture fill factors along the x axis and the y axis, respectively (Fig. 2*A* and *SI Appendix*, section *c*). A line beam then forms in the focal plane ($\alpha_x \ll 1$, $\alpha_y \sim 1$) and numerical simulations show that the peak intensity shifts toward the focusing lens for a decreasing fill factor α_y (*SI Appendix*, Fig. S2). The intensity in the focal region was imaged using two-photon fluorescence excitation of a dye solution with a near-infrared ($\lambda = 800$ nm) femtosecond Gaussian laser beam (Fig. 2*A* and *SI Appendix*, Fig. S3*A*). The fluorescence peak in the xz plane does shift toward the objective as the slit width decreases (Fig. 2*B*), while the full width at half maximum (FWHM) of the axial fluorescence profile increases. We also observed a skewed axial intensity profile at low y apertures, in agreement with previous experiments made with circular apertures (4–6, 14), but we found a comparatively larger focal shift and axial FWHM (*SI Appendix*, Fig. S4). In this experiment, $\mathcal{N}_x = 0.034$ while $\mathcal{N}_y$ decreases from 850 to 108 ($0.88 > \alpha_y > 0.31$). The numerical integration of the scalar diffraction integral using a Gaussian elliptical beam clipped in the y direction gave a reasonable fit with experimental values of the focal shift and the axial FWHM (Fig. 2*B*).

Focal Shift in Temporal Focusing

To further explore focal shift for nonaxially symmetric focusing, we also considered another kind of focusing known as temporal focusing (27, 28, 31), a technique that is increasingly used for biological imaging (32–34) but introduces a new wave asymmetry due to a spectral dispersion along one axis. Here ultrashort femtosecond pulses are first spectrally spread in the x direction and then refocused by the imaging objective to gradually overlap and maximally interfere in the so-called temporal focusing plane (Fig. 2*C*), where the ultrashort pulse duration is restored (27). To the best of our knowledge, focal shift has been studied only in the monochromatic case and not for temporal focusing. Practically, we focused a femtosecond laser beam (bandwidth $\Omega = 40$ nm) on the objective back aperture as a small circular beamlet (radius $a_0 = 22$ μm), but also spectrally dispersed it along the x axis (0.2 mm/nm) to create a rainbow of beamlets. A slit controls the spatial extension of that rainbow (Fig. 2*C* and *SI Appendix*, Fig. S3*B*). The two-photon–induced fluorescence produced in the focal region appears as a line in the xz plane. When reducing the x aperture, the fluorescence distribution spreads along the z axis and shifts toward the objective (Fig. 2*D*). The tendency and magnitude are similar to classical focusing (spatial focusing) from an elliptical beam (*SI Appendix*, Fig. S5). This experiment was modeled by introducing a spectral dispersion into the diffraction integral together with two Fresnel numbers, $\mathcal{N}_T = (a_x^2 + \alpha^2\Omega^2)/\lambda f$ in the temporal x direction and $\mathcal{N}_S = a_y^2/\lambda f$ in the spatial y direction with $a_x = a_y = a_0$ (Fig. 2*D* and *SI Appendix*, section *d*). Here, $\mathcal{N}_S = 0.034$, while $108 \le \mathcal{N}_T \le 850$ ($0.31 < \alpha_x < 0.88$).

Focal Shift and Axial Resolution in Line-Temporal Focusing

In the field of high-resolution and fast optical imaging, line-temporal focusing microscopy (LTFM) (also called spatiotemporal focusing) is an attractive method for deep bioimaging, in which wave focusing is strongly asymmetric with distinct focusing processes in the perpendicular spatial and temporal directions (28, 35). Since we found focal shifts with similar magnitudes for elliptical spatial focusing and temporal focusing of a rainbow ellipse (Fig. 2 and *SI Appendix*, Fig. S5), two distinct focal shifts can be reasonably expected if the spectral and the spatial apertures are different. The expected gap Δf_{xy} between the temporal focal plane (TFP) and the spatial focal plane (SFP) (Fig. 3*A*) could compromise the axial resolution. A heuristic evaluation of that gap is proposed (*SI Appendix*, section *e*), but it is an unsolved and difficult problem to evidence such a gap theoretically and experimentally.

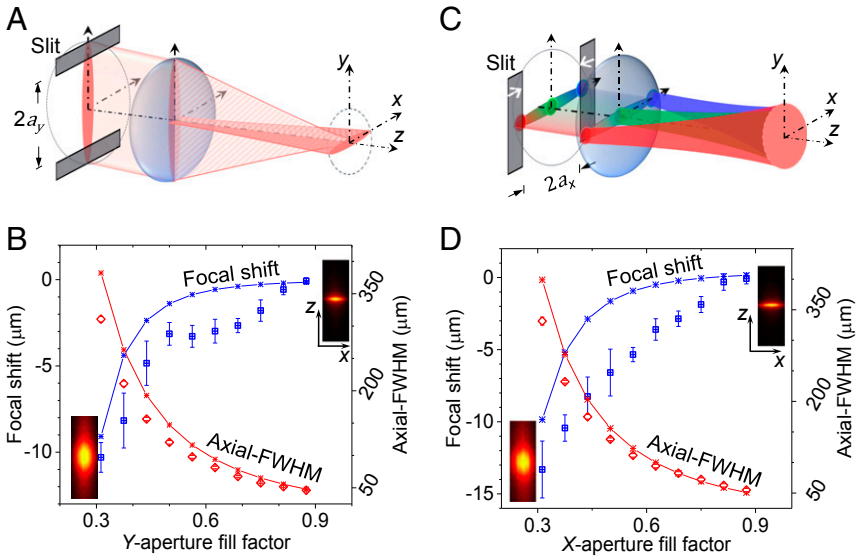

Fig. 2. Focal shift in noncircular aperture focusing. (*A* and *B*) Noncircular spatial focusing. The laser beam is first focused by a cylindrical lens to an elliptical beam spot with size 2 × 22 μm along the x axis and 7 mm along the y axis that is subsequently focused by an objective lens (10× NA = 0.3). (*C* and *D*) Temporal focusing. The femtosecond laser spectrum is first spread by a grating and focused by a spherical lens to form a rainbow line along the x axis, of circular beamlets with diameter 44 μm, producing temporal focusing along the x axis. Experimental and theoretical data (*SI Appendix*, sections *c* and *d*) show the focal shifts (blue squares) and axial FWHMs (red diamonds) when focused with different aperture sizes for spatial (*B*) and temporal (*D*). The focal shifts (blue squares) and the axial FWHM (red diamonds) of fluorescence profiles for experiments and theoretical data are shown by solid lines. *B* and *D*, *Insets* display the fluorescence zx images in noncircular spatial focusing and temporal focusing, respectively.

To directly assess how spatial and temporal focal shifts contribute to the axial intensity profile when combined, we introduced extraneous group velocity dispersion (GVD) in the laser pulses to shift the temporal focal plane in a controlled manner as already known (*SI Appendix*, section *f* and Fig. S6). With a large enough GVD, a bimodal axial fluorescence intensity profile was obtained, with a significant gap Δf between the TFP and the SFP (*SI Appendix*, Fig. S7). Interestingly, given a fixed amount of GVD used to set the TFP, the amplitude of the aperture-induced shift of the SFP did not depend on the GVD value. This suggests that the focal shifts in these two directions contribute independently of each other. In other words, the aperture fill factors α_x and α_y used in LTFM seem to determine the temporal and spatial focusing independently (Fig. 3*B*). However, when the spatial *y* aperture was kept constant ($\alpha_y = 0.88$) while reducing temporal fill factor α_x from 0.88 to 0.19, the peak position first shifted toward the objective lens, reached a maximum shift at around $\alpha_x = 0.60$, but returned to the SFP when further decreasing α_x (Fig. 3*B*, black open squares). This nonmonotonic behavior agrees qualitatively well with our simulation (Fig. 3*B*, blue open circles). The axial FWHM increases monotonically when α_x decreases (Fig. 3*B*), showing that a reduced temporal focusing aperture degrades the axial resolution previously thought to be set by the aperture of spatial focusing. A similar effect is seen when reducing the spatial fill factor (*SI Appendix*, Fig. S8). The nonmonotonic behavior seen for the focal shift can be interpreted as follows. Initially, similar contrasts are produced for similar apertures, and the shift of contrast produced by the decreasing aperture does cause a global shift. However, as the decreasing aperture is further reduced, the corresponding contrast vanishes and no longer contributes to the global shift.

Optimizing Resolution in LTFM

Based on these ideas, we assessed how much the axial resolution of LTFM can be improved by restoring the circular symmetry of the aperture. A multimodal instrument with alternative modalities was built (*SI Appendix*, Fig. S9), namely LTFM and two-photon point scanning microscopy (PSM). A femtosecond laser with central wavelength 800 nm, repetition rate 80 MHz, and 36 nJ/pulse was used for photoexcitation; a water-immersion 10× NA 0.45 objective was used for focusing (*Materials and Methods*). As expected, the axial resolution of LTFM is improved significantly by more circular filling of the objective aperture and/or increasing the laser spectral width of Ω (*SI Appendix*, section *g* and Figs. S10–S12 and S13 *A* and *B*), up to the point where it beats the axial resolution obtained with PSM. For broad spectra ($\Omega \geq 21.4$ nm), it reaches nearly the theoretical resolution of PSM (36), which is remarkable as this limit is practically never reached in any other experiments.

Axial intensity profiles further demonstrate that LTFM, when optimized, exhibits better axial resolution than PSM (Fig. 3*C* and *SI Appendix*, Figs. S3*C* and S12). When imaging deep into a thick biological sample (fluorescently labeled mouse lung; *Materials and Methods*), LTFM with a circularly filled back aperture significantly improves the axial resolution and contrast to become better than PSM, with detectable signal beyond a 900-μm depth (Fig. 3*D*). In other words, we find that LTFM, as a wide-field detection method, is not only significantly faster but also better resolved than PSM.

Historical Context

The introduction by Wolf (1) and Richards and Wolf (2) of the first full integral vectorial representation of the image field represents a landmark contribution to our understanding of wave

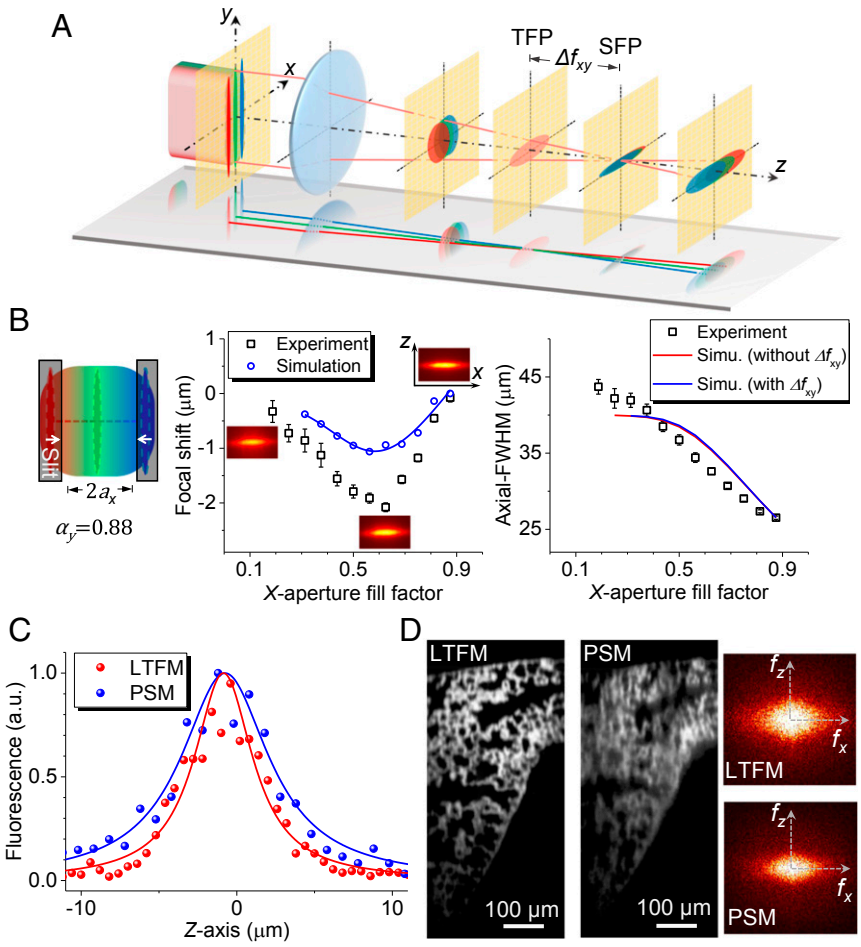

Fig. 3. Focal shifts in LTFM. (*A*) Schematic representation of line-temporal focusing. The polychromatic beam with spectrum spread by a grating is focused by a cylindrical lens along the *x* axis through an objective lens. Spatial and temporal focusing in the *zy* and the *zx* plane, respectively, lead to an SFP and a TFP. (*B*) The focal shifts and axial FWHMs are shown as a function of the temporal aperture and analyzed with the arguments in *SI Appendix*, section *d*. *Insets* display the fluorescence *xz* images in line-temporal focusing. (*C*) Axial fluorescence profiles of LTFM and PSM. (*D*) *xz* images of a mouse lung slice in the same region by LTFM and PSM; *D*, *Right* shows 2D Fourier transforms of these *xz* sections.

focusing. This new theory, developed for axially symmetric and aplanatic focusing, combined the Debye approximation of a truncated angular spectrum in the aperture plane, with an approximate Kirchhoff boundary condition such that no inclination factor was needed. Compared with the vectorial Fresnel–Kirchhoff diffraction theory, it was intrinsically more suitable for large-aperture angles, and it proved very successful to compute the vectorial diffraction integrals, to describe the vectorial properties of focused light (polarization and Poynting vector) and the geometry of the energy flow (20, 37).

However, difficulties with this theory have been noted over the years. Indeed, the same report by Collett and Wolf (ref. 38, p. 264) that predicts the inversion symmetry of the optical field and the antisymmetry of its phase relative to the focal plane also states that this prediction raises a fundamental issue of consistency:

> Although such symmetries follow formally from the analytic solutions ... they are not self-evident physically; for focused fields seem to be intrinsically asymmetric because the field converges toward the focal region on one side of the focal plane and diverges on the other. It is not clear, a priori, why diffraction should not destroy the symmetry that might perhaps be expected according to some quasi-geometrical arguments.

This symmetry problem had indeed been an issue since experimental evidence was published in the 1950s and 1960s showing that the focus of microwaves did not correspond to the geometric focus, i.e., to the center of curvature of wavefronts (39, 40). With the new technology of lasers, similar effects were observed experimentally in the 1960s with light [Gusinow et al. (4) and Kogelnik (41)]. Although early experiments dealt with Gaussian beams, the notion of focal shift was first introduced by Osterberg and Smith (3) for scalar spherical waves. In the latter report, the first Rayleigh–Sommerfeld integral was used to show that the peak axial intensity does not sit at the center of curvature of the waves, but rather in a plane closer to the aperture plane. A similar theoretical observation was later made by Holmes et al. (8) and Heurtley (9), with a clear agreement between experiments and theory (4), and the notion of a retrograde focal shift for Gaussian beams is now a textbook fact (42). Interestingly, the Gouy phase pattern also exhibits a retrograde shift by the same amount and is no longer antisymmetric with respect to the nominal focus. For Gaussian acoustic beams, this symmetry breaking of the intensity and the Gouy phase relative to the nominal focus was observed and theoretically explained in the early 1980s (43) and later (44).

In the early 1980s, an outstanding problem was to bridge Wolf's theory (1, 2) that failed to catch the consequences of the fundamental breaking of the forward–backward symmetry about the focal plane, with scalar diffraction theories based on the Kirchhoff assumption and the Rayleigh–Sommerfeld integrals (3, 9) that failed to work for large aperture and vector fields. In this context, key papers by Stamnes (11) and Stamnes and Spjelkavik (12) suggested two methods to improve the core Debye assumption of Wolf's theory, i.e., the blunt truncation of the angular spectrum, which amounts to neglecting boundary diffraction by abruptly cutting away all components with an angle larger than the aperture angle. Using the Kirchhoff assumption to introduce a smoother angular spectrum, Stamnes could demonstrate that, even for large-aperture angles, the Kirchhoff assumption of an abruptly vanishing field at the aperture boundary does better than the Debye assumption of an abruptly vanishing angular spectrum (11, 12). This new viewpoint breaks the inversion symmetry about the focus, because it takes boundary diffraction into account. Soon after these important contributions from Stamne, and "in order to clarify this situation" (ref. 45, p. 205), Wolf proposed that his Debye integral representation should be considered only beyond a critical value of the Fresnel number (45), computed this critical value, and proposed a new theory for the focal shift effect (10, 13), based on his earlier work on boundary diffraction (46, 47).

A rather limited series of experimental papers was then published that were dedicated to focal shift for 3D waves or Gaussian beams focused under low Fresnel number conditions ($\mathcal{N} < 10$) (5–7). Since 1984, we are not aware of any experimental report on focal shift per se, except in acoustics (44) and plasmonics (17, 18). In optics, very few experimental contributions related to light focal shift were published, showing that it could be compensated by introducing well-controlled aberration (48) or modulating the degree of spatial coherence of the focused wave (49).

Concluding Remarks

The simple symmetry arguments developed in this paper explain why the focus of an aberration-free wave must shift toward the focusing lens and why the breaking of the circular symmetry of the aperture or beam section per se should lead to astigmatic focusing and stretching of the axial intensity profile. Beyond the very few experimental reports on focal shift, this phenomenon is explored here for noncircular apertures and beam sections experimentally. Its amplitude as a function of a bidirectional set of two Fresnel numbers is found to be similar for the spatial and temporal focusing of an elliptical femtosecond beam. The contribution of the beam asymmetry to focal shift is best reflected by the fact that the amplitude of the shift of a line-temporal focus is a nonmonotonic function of the aspect ratio of the beam (Fig. 3*B*). Our demonstration that the restoration of an effective aperture symmetry improves the axial resolution of LTFM beyond the resolution of the classical two-photon PSM strongly suggests that methods based on focusing waves from asymmetric apertures could suffer from an intrinsic limit of their axial resolution because of the aperture-induced astigmatism.

The practical impact of our findings for the design of focusing devices can be discussed as follows. Unlike theory which can handle perfectly spherical waves or Gaussian beams, experiments must deal with spherical aberrations that also entail an extrinsic focal shift which is difficult to tell from the intrinsic focal shift studied here. Both focal shifts add, but telling them apart may be practically unimportant, because intrinsic shift can be satisfactorily compensated by well-tuned extraneous aberration as shown for monochromatic light. However, as noted above for an increasing number of nonconventional large-aperture focusing devices, focal shift must be considered not only to best locate the focus, but also to optimize the axial resolution, with the possibility to compensate aperture-induced astigmatism by nonspherical geometric corrections of the beam or of the focusing optics. However, to optimize the wide range of applications based on wave focusing, further theoretical developments are much needed to quantitatively understand the underlying physics.

Materials and Methods

Setup for Elliptical Spatial Focusing and Temporal Focusing. The pulsed output of a femtosecond laser (Vitara; Coherent Inc.) with central wavelength 800 nm, repetition rate 80 MHz, and 10 nJ/pulse was shaped using a telescope to an 8-mm–waist collimated beam, and its power was controlled by an achromatic half-wave plate followed by a polarizer. It was subsequently reflected by a blazed grating (600/mm) or a reflecting mirror and collected by a cylindrical lens or a spherical lens with the same 300-mm focal length for both options (*SI Appendix*, Fig. S3). The beam size was controlled close to the back aperture of the focusing objective by a 2D slit composed of two orthogonal mechanical slits (VA100; Thorlabs). The laser pulses were focused by an air objective lens (10× NA 0.3; Zeiss) into a cuvette sealed with a cover glass and filled with a 1-mM aqueous solution of rhodamine B. The fluorescence emission was collected by a perpendicular objective lens (20× NA 0.5; Olympus) and imaged through a tube lens (TTL200; Thorlabs) and an emission filter (ET600/50m; Semrock) onto an EMCCD (iXon 888; Andor).

LTFM. A femtosecond laser with a central wavelength of 800 nm and an 80-MHz repetition rate was used (Mai-Tai; Spectra-Physics). Maximum intensity pulses were obtained at 800 nm, with 36 nJ energy per pulse and pulse durations of 110 fs ($\Omega \sim 9.4$ nm) measured with an autocorrelator (FR-103XL; Femtochrome Research Inc.). The laser power was controlled by an achromatic half-wave plate and a Faraday isolator FI (EOT Inc.). The laser spectrum was measured with a fiber spectrometer (USB4000; Ocean-Optics Inc.). After the isolator, a dispersion precompensation prism pair (SF10 glass; Thorlabs Inc.) was inserted, followed by a 3× telescope T. The expanded beam impinged on a phase-only spatial light modulator (SLM) (X10468-02; Hamamatsu Photonics) as a 10-mm diameter disk, with a small incident angle (4.3°). After the SLM, an afocal

cylindrical lens (CL) pair was inserted (CL1 and CL2, $f_{CL1} = 400$ mm, $f_{CL2} = 500$ mm). At the back focal plane of CL2, the beam was reflected from a 1D galvanometric mirror (GM1; Thorlabs Inc.) and focused through a cylindrical lens (CL3, $f_C = 500$ mm) as a 20-mm–long line onto the surface of a 1,200 line/mm blazed grating G (GR50-1208; Thorlabs Inc.). The spectral components dispersed by the grating were collected by a spherical collimating lens (L_C, $f_L = 500$ mm) onto the back aperture of a water-immersion objective lens (10×, NA 0.45). The fluorescence emission passes through the objective, a tube lens, and an emission filter before being detected by an EMCCD (iXon 897; Andor) (*SI Appendix*, Fig. S9). While the GM1 mirror typically oscillates with a triangular wave at 800 Hz, the camera was typically operated at 10 frames per second.

Home-Built Two-Photon PSM. As shown in *SI Appendix*, Fig. S9, the two-photon PSM branch connects to the LTFM setup by a mirror located after the SLM and starts with an afocal pair of spherical lenses (L2, $f_{L2} = 400$ nm and L3, $f_{L3} = 500$ mm) followed by a 2D galvanometric mirror (GM2) (GVS012; Thorlabs). The mirror plane is conjugate to the objective back aperture by a conventional 4*f* system (L3 and L4, $f_L = 500$ mm). To compare the axial FWHMs between the two-photon PSM and the LTFM, the same EMCCD was used. The GM1 mirror was driven by a triangular wave voltage, typically operated at 800 Hz. Z scanning was done by automatically moving the objective lens. Image stacks were captured using the ZEN 2012 program (Zeiss). Axial FWHM was assessed using fluorescent beads trapped in agarose hydrogels and by fitting their vertical intensity profiles with the Cauchy–Lorentz function.

Intracavity Laser Spectrum Modulation. The initial spectrum from the ultrafast oscillator (Mai-Tai; Spectra-Physics) has a narrow spectrum, FWHM = 9.4 nm. By controlling the angles of the intracavity prism pair and the width of the mode-locking aperture, the pulse spectrum could be tuned from 6.6 nm to 21.4 nm.

Measurements of Fluorescence in LTFM. Axial fluorescence profiles were taken by using fluorescent beads with 0.5 μm diameter (F8812; Life Technologies) diluted in deionized water to 1:2,000. Bead suspensions were then further diluted (1.5:100) in agarose (BP 160-100; Fisher Scientific) and then filled into a mounting slide with controlled thickness (635021; Grace Bio-Labs).

Biological Sample Preparation and Imaging. Mouse (Swiss Webster) lungs were dissected in adherence to the Animal Welfare Act and the Public Health Service Policy on Humane Care and Use of Laboratory Animals; all experiments with and care of mice were performed in accordance with protocols approved by the Institutional Animal Care and Use Committees (IACUC) of Stanford University (protocol approval number 30366). Samples were fixed in 4% formaldehyde supplemented with 1% Nonidet P-40, 0.2% Triton X-100, 4% acrylamide, and 0.25% photoinitiator (VA-044; Wako Chemicals) for 24–48 h. After fixation, polymerization of acrylamide was initiated by exchanging all gas with nitrogen and the polymerization was allowed to proceed for 1–2 h at 37 °C before the fixative was removed. This polymerization step allows forming a polymer matrix around the tissue to support the porous structure of the lung which otherwise often collapses. The lung tissue was bleached in 6% H_2O_2 in PBS for 16 h overnight under strong light and the bleaching solution was removed by extensive washing in PBS supplemented with 0.3% Triton X-100 and 4% SDS at 37 °C. The bleached tissue was then stained with rhodamine- or fluorescein-labeled peanut agglutinin (PNA; Vector Labs) following the procedure recommended by the manufacturer.

ACKNOWLEDGMENTS. We thank Prof. Bo Wang (Stanford University) for providing us with fixed mouse lung samples and his participation in early stages of this study. We thank Guillaume Graciani and Ah-Young Jee for discussions. This work was supported by the taxpayers of South Korea through the Institute for Basic Science, Project IBS-R020-D1.

1. Wolf E (1959) Electromagnetic diffraction in optical systems. I. An integral representation of the image field. *Proc R Soc A* 253:349–357.
2. Richards B, Wolf E (1959) Electromagnetic diffraction in optical systems. II. Structure of the image field in an aplanatic system. *Proc R Soc A* 253:358–379.
3. Osterberg H, Smith LW (1961) Closed solutions of Rayleigh's diffraction integral for axial points. *J Opt Soc Am* 51:1050–1054.
4. Gusinow MA, Riley ME, Palmer MA (1977) Focusing in a large F-number optical system. *Opt Quantum Electron* 9:465–471.
5. Li Y (1983) Encircled energy of diffracted converging spherical waves. *J Opt Soc Am* 73:1101–1104.
6. Li Y, Platzer H (1983) An experimental investigation of diffraction patterns in low-Fresnel-number focusing systems. *Opt Acta* 30:1621–1643.
7. Sucha GD, Carter WH (1984) Focal swift for a Gaussian beam: An experimental study. *Appl Opt* 23:4345–4347.
8. Holmes DA, Korka JE, Avizonis PV (1972) Parametric study of apertured focused Gaussian beams. *Appl Opt* 11:565–574.
9. Heurtley JC (1973) Scalar Rayleigh–Sommerfeld and Kirchhoff diffraction integrals: A comparison of exact evaluations for axial points. *J Opt Soc Am* 63:1003–1008.
10. Li Y, Wolf E (1981) Focal shifts in diffracted converging spherical waves. *Opt Commun* 39:211–215.
11. Stamnes JJ (1981) Focusing of two-dimensional waves. *J Opt Soc Am* 71:15–31.
12. Stamnes JJ, Spjelkavik B (1981) Focusing at small angular apertures in the Debye and Kirchhoff approximations. *Opt Commun* 40:81–85.
13. Li Y (1982) Dependence of the focal shift on Fresnel number and F-number. *J Opt Soc Am* 72:770–774.
14. Stamnes JJ (1986) *Waves in Focal Regions: Propagation, Diffraction, and Focusing of Light, Sound, and Water Waves* (A Hilger, Bristol, UK).
15. Li Y (2005) Focal shifts in diffracted converging electromagnetic waves. I. Kirchhoff theory. *J Opt Soc Am A Opt Image Sci Vis* 22:68–76.
16. Lee JY, et al. (2009) Near-field focusing and magnification through self-assembled nanoscale spherical lenses. *Nature* 460:498–501.
17. Gao Y, et al. (2012) Analysis of focal-shift effect in planar metallic nanoslit lenses. *Opt Express* 20:1320–1329.
18. Yu Y, Zappe H (2012) Theory and implementation of focal shift of plasmonic lenses. *Opt Lett* 37:1592–1594.
19. Chmyrov A, et al. (2013) Nanoscopy with more than 100,000 'doughnuts'. *Nat Methods* 10:737–740.
20. Boivin A, Dow J, Wolf E (1967) Energy flow in the neighborhood of the focus of a coherent beam. *J Opt Soc Am* 57:1171–1175.
21. Tokunaga M, Imamoto N, Sakata-Sogawa K (2008) Highly inclined thin illumination enables clear single-molecule imaging in cells. *Nat Methods* 5:159–161.
22. Trache A, Meininger GA (2017) Total internal reflection fluorescence (TIRF) microscopy. *Curr Protoc Microbiol* 10:2A.2.1–2A.2.22.
23. Yang B, Przybilla F, Mestre M, Trebbia JB, Lounis B (2014) Large parallelization of STED nanoscopy using optical lattices. *Opt Express* 22:5581–5589.
24. Sheppard CJR (2007) The optics of microscopy. *J Opt A Pure Appl Opt* 9:S1–S6.
25. Li YJ (1988) Focusing non-truncated elliptical Gaussian beams. *Opt Commun* 68:317–323.
26. Chen BC, et al. (2014) Lattice light-sheet microscopy: Imaging molecules to embryos at high spatiotemporal resolution. *Science* 346:1257998.
27. Oron D, Tal E, Silberberg Y (2005) Scanningless depth-resolved microscopy. *Opt Express* 13:1468–1476.
28. Tal E, Oron D, Silberberg Y (2005) Improved depth resolution in video-rate line-scanning multiphoton microscopy using temporal focusing. *Opt Lett* 30:1686–1688.
29. Yan Z, Sajjan M, Scherer NF (2015) Fabrication of a material assembly of silver nanoparticles using the phase gradients of optical tweezers. *Phys Rev Lett* 114:143901.
30. Lozano C, Ten Hagen B, Löwen H, Bechinger C (2016) Phototaxis of synthetic microswimmers in optical landscapes. *Nat Commun* 7:12828.
31. Durst ME, Zhu G, Xu C (2006) Simultaneous spatial and temporal focusing for axial scanning. *Opt Express* 14:12243–12254.
32. Dana H, Kruger N, Ellman A, Shoham S (2013) Line temporal focusing characteristics in transparent and scattering media. *Opt Express* 21:5677–5687.
33. Papagiakoumou E, et al. (2013) Functional patterned multiphoton excitation deep inside scattering tissue. *Nat Photonics* 7:274–278.
34. Schrödel T, Prevedel R, Aumayr K, Zimmer M, Vaziri A (2013) Brain-wide 3D imaging of neuronal activity in Caenorhabditis elegans with sculpted light. *Nat Methods* 10:1013–1020.
35. Dana H, Shoham S (2012) Remotely scanned multiphoton temporal focusing by axial grism scanning. *Opt Lett* 37:2913–2915.
36. Zipfel WR, Williams RM, Webb WW (2003) Nonlinear magic: Multiphoton microscopy in the biosciences. *Nat Biotechnol* 21:1369–1377.
37. Boivin A, Wolf E (1965) Electromagnetic field in the neighborhood of the focus of a coherent beam. *Phys Rev* 138:B1561–B1565.
38. Collett E, Wolf E (1980) Symmetry properties of focused fields. *Opt Lett* 5:264–266.
39. Bachynski MP, Bekefi G (1957) Study of optical diffraction images at microwave frequencies. *J Opt Soc Am* 47:428–438.
40. Farnell GW (1958) On the axial phase anomaly for microwave lenses. *J Opt Soc Am* 48:643–647.
41. Kogelnik H (1965) On the propagation of Gaussian beams of light through lenslike media including those with a loss or gain variation. *Appl Opt* 4:1562–1569.
42. Lipson A, Lipson H, Lipson SG (2010) The scalar theory of diffraction. *Optical Physics* (Cambridge Univ Press, Cambridge,UK), 4th Ed, pp 198–226.
43. Thompson RB, Lopes EF (1984) The effects of focusing and refraction on Gaussian ultrasonic beams. *J Nondestr Eval* 4:107–123.
44. Makov YN, Sánchez-Morcillo VJ, Camarena F, Espinosa V (2008) Nonlinear change of on-axis pressure and intensity maxima positions and its relation with the linear focal shift effect. *Ultrasonics* 48:678–686.
45. Wolf E, Li Y (1981) Conditions for the validity of the Debye integral-representation of focused fields. *Opt Commun* 39:205–210.
46. Miyamoto K, Wolf E (1962) Generalization of the Maggi-Rubinowicz theory of the boundary diffraction wave—Part I. *J Opt Soc Am* 52:615–625.
47. Miyamoto K, Wolf E (1962) Generalization of the Maggi-Rubinowicz theory of the boundary diffraction wave—Part II. *J Opt Soc Am* 52:626–636.
48. Jiang DY, Stamnes JJ (1997) Theoretical and experimental results for focusing of two-dimensional scalar waves. *Pure Appl Opt* 6:211–224.
49. Wang F, Cai YJ, Korotkova O (2009) Experimental observation of focal shifts in focused partially coherent beams. *Opt Commun* 282:3408–3413.